

Comparison of in- and out-of-plane charge dynamics in $\text{YBa}_2\text{Cu}_3\text{O}_{6.95}$

E. Schachinger

Institut für Theoretische Physik, Technische Universität Graz

A-8010 Graz, Austria

J.P. Carbotte

Department of Physics and Astronomy, McMaster University,

Hamilton, Ont. L8S 4M1, Canada

(November 1, 2018)

Abstract

The in-plane optical conductivity has been successfully employed to obtain information about the coupling of the charge carriers to the spin degrees of freedom in the high T_c oxides. We investigate how this inelastic scattering affects the out of plane charge dynamics. We consider both coherent (in-plane momentum is conserved) and incoherent (no momentum conservation) c -axis transfers and find that the two cases give quite a distinct c -axis conductivity as a function of energy ω . Comparison of our theoretical calculations with the available data does not allow a definitive conclusion, but a momentum dependent coherent matrix element characteristic of the CuO_2 chemistry is favored with the possibility of a subdominant incoherent contribution.

74.20.Mn 74.25.Gz 74.72.-h

I. INTRODUCTION

Carbotte *et al.*¹ recently suggested that a signature of the 41 meV spin resonance which is measured in spin polarized inelastic neutron scattering experiments² in the superconducting state of optimally doped $\text{YBa}_2\text{Cu}_3\text{O}_{6.95}$ (YBCO), is also seen in the in-plane infrared optical spectrum as a function of energy ω . Following this initial suggestion Schachinger and Carbotte^{3,4} proceeded to analyze optical spectra in other high- T_c compounds and found that similar spin resonances develop in many of the cuprates but not in all. These authors provided a simple technique^{1,3-6} to extract from infrared data an approximate electronic carrier-spin fluctuation spectral density which not only gives a picture of the position and width of the spin resonance, but also gives an absolute measure of its coupling to the charge degrees of freedom. More recently, consideration of in-plane optical data⁷ in YBCO at several temperatures reproduced well the temperature evolution of the 41 meV resonance⁸ measured in neutron scattering experiments and gave a carrier-spin fluctuation spectral density which showed considerable variation with temperature. It consists of a broad spin fluctuation background which extends, in frequency, to several hundred millivolts and which persists in the normal state. Superimposed on this background is a spin resonance contribution which exists only in the superconducting state for optimally doped YBCO and grows as T is lowered. The growth of the resonance reflects modifications to the spin spectrum connected with the development of the superconducting state as the temperature is lowered below T_c (the superconducting critical temperature). It is found that feedback effects increase the stability of superconductivity and, within an Eliashberg formalism for the superconducting state, lead directly to a ratio of the d -wave gap amplitude to the value of T_c which is considerably larger⁹ than the BCS value of 4.3 in agreement with experiment.

Other observed properties of the superconducting state can also be understood directly within the same framework. Most prominent among these are (1) agreement with experiment for the value of the zero temperature condensation energy per copper atom,^{10,11} (2) the fact that only about one third of the total optical spectral weight condenses into the superfluid density at zero temperature.¹² This arises because it is mainly the coherent part of the charge

carrier spectral density which condenses while the incoherent boson assisted background is largely unaffected by the condensation. (3) The large peak observed in the microwave conductivity around 35 K¹³ is understood as due to the collapse of the electronic scattering rates¹⁴ which results from a low frequency gapping of the spin fluctuation spectrum due to the onset of superconductivity. (4) There is also a corresponding peak in the thermal conductivity which the calculations explain.¹⁵

In this paper we wish to extend the work to the c -axis optical conductivity^{16–18} to see if it too can be satisfactorily understood within a generalized Eliashberg formalism with kernels determined from in-plane optical conductivity data.¹⁹ The out-of-plane optical response has been the subject of considerable recent interest^{20–28} due in part to the observation of an important violation of the conventional Ferrell-Grover-Tinkham²⁹ (FGT) sum rule. This sum rule is obeyed by conventional superconductors but not by some high T_c cuprates in the direction perpendicular to the CuO₂ planes. In this case the missing spectral weight under the real part of the optical conductivity which disappears on entering the superconducting state, does not necessarily equal the superfluid density which condenses into a delta function at zero frequency $\omega = 0$ in the real part of the optical conductivity. In this paper we will concentrate on the frequency dependence of the c -axis optical conductivity $\sigma_c(T, \omega)$ at low temperatures T in the superconducting state for $\omega > 0$.

II. FORMALISM

The out-of-plane conductivity $\sigma_c(T, \omega)$ at temperature T and frequency ω is related to the current-current correlation function $\Pi_c(T, i\nu_n)$ at the boson Matsubara frequency $\nu_n = 2n\pi T$, $n = 0, \pm 1, \pm 2, \dots$, analytically continued to real frequency ω , and to the c -axis kinetic energy $\langle H_c \rangle$:^{25,34}

$$\sigma_c(T, \omega) = \frac{1}{\omega} \left[\Pi_c(T, i\nu_n \rightarrow \omega + i0^+) - e^2 d^2 \langle H_c \rangle \right], \quad (1)$$

with e the charge on the electron and d the distance between planes in the c -direction. In terms of the in-plane thermodynamic Green's function $\hat{G}(\mathbf{k}, i\omega_n)$ and for coherent hopping

$t_{\perp}(\mathbf{k})$ perpendicular to the CuO_2 planes

$$\Pi_c(T, i\nu_n) = 2(ed)^2 T \sum_{\omega_m} \sum_{\mathbf{k}} t_{\perp}^2(\mathbf{k}) \text{tr} \left\{ \hat{\tau}_0 \hat{G}(\mathbf{k}, i\omega_m) \hat{\tau}_0 \hat{G}(\mathbf{k}, i\omega_m + i\nu_n) \right\} \quad (2a)$$

and

$$\langle H_c \rangle = 2T \sum_{\omega_m} \sum_{\mathbf{k}} t_{\perp}^2(\mathbf{k}) \text{tr} \left\{ \hat{\tau}_3 \hat{G}(\mathbf{k}, i\omega_m) \hat{\tau}_3 \hat{G}(\mathbf{k}, i\omega_m) \right\} \quad (2b)$$

In Eqs. (2) the 2×2 Nambu Green's function $\hat{G}(\mathbf{k}, i\omega_m)$ describes the in-plane dynamics of the charge carriers with momentum \mathbf{k} in the two dimensional CuO_2 plane Brillouin zone, $i\omega_n = i(2n + 1)\pi T$ for temperature T , $n = 0, \pm 1, \pm 2, \dots$, and is given by

$$\hat{G}(\mathbf{k}, i\omega_n) = \frac{i\tilde{\omega}(i\omega_n)\hat{\tau}_0 + \zeta_{\mathbf{k}}\hat{\tau}_3 + \tilde{\Delta}_{\mathbf{k}}(i\omega_n)\hat{\tau}_1}{-\tilde{\omega}^2(i\omega_n) - \zeta_{\mathbf{k}}^2 - \tilde{\Delta}_{\mathbf{k}}^2(i\omega_n)}, \quad (3)$$

where the $\hat{\tau}$'s are the Pauli 2×2 matrices, $\zeta_{\mathbf{k}}$ is the band energy of the charge carriers as a function of their momentum \mathbf{k} , $\tilde{\Delta}_{\mathbf{k}}(i\omega_n)$ is the renormalized gap and $\tilde{\omega}(i\omega_n)$ the renormalized Matsubara frequencies. In our model these quantities are determined as solutions of Eliashberg equations suitably generalized to describe a d -wave superconductor in terms of a charge carrier-spin fluctuation spectral density $I^2\chi(\omega)$ which we have determined previously from consideration of the in-plane optical conductivity.^{1,3,4} The method^{1,3-7} is to use the second derivative $\frac{1}{2\pi} \frac{d^2}{d\omega^2} [\omega\tau^{-1}(\omega)]$ of the optical scattering rate $\tau^{-1}(\omega)$ in the superconducting state as a first estimate in the construction of a model for the underlying charge carrier - spin fluctuation spectral density $I^2\chi(\omega)$.

In Eqs. (2) the out-of-plane matrix element $t_{\perp}(\mathbf{k})$ can depend on the in-plane momentum \mathbf{k} . Models have been summarized in the recent preprint of Sandeman and Schofield³⁰ who refer to previous literature.³¹⁻³³ A possible choice is $t_{\perp}(\mathbf{k}) = t_{\perp}$, a constant. But, consideration of the chemistry of the CuO_2 plane and of the overlap of one plane with the next, suggests a form $t_{\perp}(\mathbf{k}) = \cos^2(2\phi)$ where ϕ is the angle of \mathbf{k} in the two dimensional CuO_2 Brillouin zone for the plane motion. This matrix element eliminates the contribution from nodal quasiparticles entirely from the c -axis motion.

For incoherent impurity induced c -axis charge transfer Eqs. (2) are to be modified. After an impurity configuration average we obtain

$$\Pi_c(T, i\nu_n) = 2(ed)^2 T \sum_m \sum_{\mathbf{k}, \mathbf{k}'} \overline{V_{\mathbf{k}, \mathbf{k}'}}^2 \left\{ \hat{\tau}_0 \hat{G}(\mathbf{k}, i\omega_m) \hat{\tau}_0 \hat{G}(\mathbf{k}, i\omega_m + i\nu_n) \right\} \quad (4a)$$

$$\langle H_c \rangle = 2T \sum_m \sum_{\mathbf{k}, \mathbf{k}'} \overline{V_{\mathbf{k}, \mathbf{k}'}}^2 \left\{ \hat{\tau}_3 \hat{G}(\mathbf{k}, i\omega_m) \hat{\tau}_3 \hat{G}(\mathbf{k}, i\omega_m) \right\}, \quad (4b)$$

with $\overline{V_{\mathbf{k}, \mathbf{k}'}}^2$ the average of the square of the impurity potential. If the impurity potential was taken to conserve momentum, which it does not, we would recover Eqs. (2). Various models could be taken for $\overline{V_{\mathbf{k}, \mathbf{k}'}}^2$. Here we use a form introduced by Kim²⁵ and Hirschfeld *et al.*¹⁸

$$\overline{V_{\mathbf{k}, \mathbf{k}'}}^2 = |V_0|^2 + |V_1|^2 \cos(2\phi) \cos(2\phi') \quad (5)$$

with ϕ and ϕ' the directions of \mathbf{k} and \mathbf{k}' respectively.

As written Eqs. (2) and (3) involve Green's functions in the imaginary frequency Matsubara representation. To obtain the conductivity $\sigma_c(T, \omega)$ as a function of real frequency an analytic continuation in Eq. (1) to real frequencies is needed. This could be done by Padé approximates, but here we analytically continue the entire equations and work with real frequency Eliashberg equations. For a d -wave superconductor with gap $\Delta_{\mathbf{k}} = \Delta_0 \cos(2\phi)$ on a cylindrical Fermi surface where ϕ is the polar angle in the two dimensional CuO₂ Brillouin zone, the basic equations for $\tilde{\Delta}$ and $\tilde{\omega}$ which include inelastic scattering due to a boson exchange mechanism between the charge carriers and described by the spectral density $I^2\chi(\omega)$ ^{35,36} take on the form

$$\begin{aligned} \tilde{\Delta}(\nu + i\delta; \phi) &= i\pi T g \sum_{m=0}^{\infty} \cos(2\phi) [\lambda(\nu - i\omega_m) + \lambda(\nu + i\omega_m)] \left\langle \frac{\tilde{\Delta}(i\omega_m; \phi') \cos(2\phi')}{\sqrt{\tilde{\omega}^2(i\omega_m) + \tilde{\Delta}^2(i\omega_m; \phi')}} \right\rangle' \\ &+ i\pi \int_{-\infty}^{\infty} dz \cos(2\phi) I^2\chi(z) [n(z) + f(z - \nu)] \left\langle \frac{\tilde{\Delta}(\nu - z + i\delta; \phi') \cos(2\phi')}{\sqrt{\tilde{\omega}^2(\nu - z + i\delta) + \tilde{\Delta}^2(\nu - z + i\delta; \phi')}} \right\rangle', \quad (6a) \end{aligned}$$

and in the renormalization channel

$$\begin{aligned} \tilde{\omega}(\nu + i\delta) &= \nu + i\pi T \sum_{m=0}^{\infty} [\lambda(\nu - i\omega_m) - \lambda(\nu + i\omega_m)] \left\langle \frac{\tilde{\omega}(i\omega_m)}{\sqrt{\tilde{\omega}^2(i\omega_m) + \tilde{\Delta}^2(i\omega_m; \phi')}} \right\rangle' \\ &+ i\pi \int_{-\infty}^{\infty} dz I^2\chi(z) [n(z) + f(z - \nu)] \\ &\times \left\langle \frac{\tilde{\omega}(\nu - z + i\delta)}{\sqrt{\tilde{\omega}^2(\nu - z + i\delta) + \tilde{\Delta}^2(\nu - z + i\delta; \phi')}} \right\rangle' + i\pi \Gamma^+ \frac{\Omega(\nu)}{c^2 + D^2(\nu) + \Omega^2(\nu)}, \quad (6b) \end{aligned}$$

with $\langle \dots \rangle$ the angular average over ϕ , and

$$\lambda(\nu) = \int_{-\infty}^{\infty} d\Omega \frac{I^2 \chi(\omega)}{\nu - \Omega + i0^+}, \quad (7)$$

$$D(\nu) = \left\langle \frac{\tilde{\Delta}(\nu + i\delta; \phi)}{\sqrt{\tilde{\omega}^2(\nu + i\delta) - \tilde{\Delta}^2(\nu + i\delta; \phi)}} \right\rangle, \quad (8)$$

$$\Omega(\nu) = \left\langle \frac{\tilde{\omega}(\nu + i\delta)}{\sqrt{\tilde{\omega}^2(\nu + i\delta) - \tilde{\Delta}^2(\nu + i\delta; \phi)}} \right\rangle. \quad (9)$$

Equations (6) are a set of nonlinear coupled equations for the renormalized pairing potential $\tilde{\Delta}(\nu + i\delta; \phi)$ and the renormalized frequencies $\tilde{\omega}(\nu + i\delta)$ with the gap

$$\Delta(\nu + i\delta; \phi) = \nu \frac{\tilde{\Delta}(\nu + i\delta; \phi)}{\tilde{\omega}(\nu + i\delta)}, \quad (10)$$

or, if the renormalization function $Z(\nu)$ is introduced in the usual way as $\tilde{\omega}(\nu + i\delta) = \nu Z(\nu)$ then

$$\Delta(\nu + i\delta; \phi) = \frac{\tilde{\Delta}(\nu + i\delta; \phi)}{Z(\nu)}. \quad (11)$$

Here, ν is a real frequency and δ is a positive infinitesimal 0^+ . To arrive at these equations a separable (in the angular part) model was used for the pairing potential. In the pairing channel it has the form $g \cos(2\phi) I^2 \chi(\omega) \cos(2\phi')$ with g a constant and $I^2 \chi(\omega)$ the pairing spectral density. This leads to a gap proportional to $\cos(2\phi)$ by arrangement. No other anisotropies are included and we note that the renormalization channel (6b) is isotropic with the same spectral density $I^2 \chi(\omega)$ as in Eq. (6a) but with no g value. In general a different form of the spectral density could come into Eqs. (6) but here, for simplicity, we have the same form but allowed for the possibility that they do not both have the same magnitude, i.e.: g needs not be equal to one. These equations are a minimum set and go beyond a BCS approach and include the inelastic scattering known to be strong in the cuprate superconductors. In the normal state at T near T_c the inelastic scattering rate varies linearly in T , as it does in our model, and is of the order of a few times T_c .

More complicated models which include the possibility of hot spots^{37–40} could be introduced in our work but would not alter the main points we wish to make. In our formalism hot spots can be introduced by inserting an angular dependent factor in Eq. (6b) for the renormalized frequencies. Presently, this quantity is isotropic but we could multiply the spectral density $I^2\chi(\omega)$ (which enters this equation) by a factor which increases the scattering in the antinodal as compared with the nodal direction. This would complicate the numerical work but goes beyond what we wish to do here. In any case, recent analysis of angular resolved photoemission (ARPES) data on the marginal Fermi liquid (MFL) phenomenology^{41–44} indicates that the inelastic part of the quasiparticle scattering in the cuprates may be quite isotropic.

For the BCS case we get similar formulas on the real axis:⁴⁵

$$\tilde{\Delta}_d(\nu, \phi) = \Delta_0 \cos(2\phi) \quad (12a)$$

$$\tilde{\Delta}_s(\nu) = i\pi t^+ \left\langle \frac{\tilde{\Delta}_s(\nu)}{\sqrt{\tilde{\omega}^2(\nu) - \tilde{\Delta}_s^2(\nu) - \tilde{\Delta}_d^2(\nu, \phi)}} \right\rangle \quad (12b)$$

$$\tilde{\omega}(\nu) = \nu + i\pi t^+ \left\langle \frac{\tilde{\omega}(\nu)}{\sqrt{\tilde{\omega}^2(\nu) - \tilde{\Delta}_s^2(\nu) - \tilde{\Delta}_d^2(\nu; \phi)}} \right\rangle, \quad (12c)$$

with impurities treated in the Born limit.

In Eq. (6b) the impurity scattering rate is proportional to Γ^+ and enters only the renormalization channel because we have assumed a pure d -wave model for the gap with zero average over the Fermi surface. This is expected to be the case in a tetragonal system. The parameter c in the elastic-scattering part of Eq. (6b) is zero for resonant or unitary scattering and infinity in the Born approximation, i.e.: weak scattering limit. In this case the entire impurity term reduces to the form $i\pi t^+ \Omega(\nu)$ with c absorbed into t^+ . For intermediate coupling c is finite. The thermal factors appear in Eqs. (6) through the Bose and Fermi distribution $n(z)$ and $f(z)$, respectively.

From the solutions of the generalized Eliashberg equations (6) we can construct the Green's function (3) analytically continued to the real frequency axis ω . In this formulation the expression for the conductivity $\sigma(T, \omega)$ based on equations (2) and (3) is lengthy; nevertheless, it is given here for completeness. For instance, the in-plane conductivity, after an

integration over \mathbf{k} has been performed, is given by:

$$\begin{aligned}
\sigma_{ab}(\Omega) &= \frac{i}{\Omega} \frac{e^2 N(0) v_F^2}{2} \\
&\times \left\langle \int_0^\infty d\nu \tanh\left(\frac{\nu}{2T}\right) \frac{1}{E(\nu; \phi) + E(\nu + \Omega; \phi)} [1 - N(\nu; \phi)N(\nu + \Omega; \phi) - P(\nu; \phi)P(\nu + \Omega; \phi)] \right. \\
&+ \int_0^\infty d\nu \tanh\left(\frac{\nu + \Omega}{2T}\right) \frac{1}{E^*(\nu; \phi) + E^*(\nu + \Omega; \phi)} [1 - N^*(\nu; \phi)N^*(\nu + \Omega; \phi) \\
&- P^*(\nu; \phi)P^*(\nu + \Omega; \phi)] + \int_0^\infty d\nu \left[\tanh\left(\frac{\nu + \Omega}{2T}\right) - \tanh\left(\frac{\nu}{2T}\right) \right] \\
&\times \frac{1}{E(\nu + \Omega; \phi) - E^*(\nu; \phi)} [1 + N^*(\nu; \phi)N(\nu + \Omega; \phi) + P^*(\nu; \phi)P(\nu + \Omega; \phi)] \\
&+ \int_{-\Omega}^0 d\nu \tanh\left(\frac{\nu + \Omega}{2T}\right) \left\{ \frac{1}{E^*(\nu; \phi) + E^*(\nu + \Omega; \phi)} [1 - N^*(\nu; \phi)N^*(\nu + \Omega; \phi) \right. \\
&- P^*(\nu; \phi)P^*(\nu + \Omega; \phi)] \\
&\left. + \frac{1}{E(\nu + \Omega; \phi) - E^*(\nu; \phi)} [1 + N^*(\nu; \phi)N(\nu + \Omega; \phi) + P^*(\nu; \phi)P(\nu + \Omega; \phi)] \right\} \Bigg\rangle \quad (13a)
\end{aligned}$$

with

$$E(\omega; \phi) = \sqrt{\tilde{\omega}_{\mathbf{k}}^2(\omega) - \tilde{\Delta}_{\mathbf{k}}^2(\omega)} \quad (13b)$$

and

$$N(\omega; \phi) = \frac{\tilde{\omega}_{\mathbf{k}}(\omega)}{E(\omega; \phi)}, \quad P(\omega; \phi) = \frac{\tilde{\Delta}_{\mathbf{k}}(\omega)}{E(\omega; \phi)}. \quad (13c)$$

In the above, $\langle \dots \rangle$ means an average over the angle ϕ and the star refers to the complex conjugate. For the c -axis conductivity $\langle \dots \rangle$ is to be replaced by $\langle \dots \cos^4(2\phi) \rangle$ and the prefactor is different with $v_F^2/2$ to be replaced by $d^2 t_\perp^2$. The above set of equations is valid for the real and imaginary part of the conductivity as a function of frequency Ω . It contains only the paramagnetic contribution to the conductivity but this is fine since we will be interested in this paper mainly in the real part of the conductivity for which the diamagnetic contribution is zero.

The real part of the incoherent conductivity along the c -axis is in turn given by (normalized to its normal state value σ_{1cn}):¹⁸

$$\frac{\sigma_{1c}(\Omega)}{\sigma_{1cn}} = \frac{1}{\nu} \int d\omega [f(\omega) - f(\omega + \Omega)] \left[N(\omega + \Omega)N(\omega) + \left| \frac{V_1}{V_0} \right| P(\omega + \Omega)P(\omega) \right]. \quad (14)$$

III. RESULTS AND DISCUSSION

We begin our discussion by highlighting some of the important results for the real part of the in-plane conductivity $\sigma_1(T, \omega)$ as a function of frequency at low temperatures T . We will want to compare our c -axis results with these in-plane results. In Fig. 1 we show $\sigma_1(\omega)$ vs. ω within BCS theory for a conventional s -wave gap (solid curve) and compare with the less known results for a d -wave superconducting gap function (dashed curve).⁴⁵ The solid curve is zero for all frequencies $\omega \leq 2\Delta_0$ (twice the s -wave gap value of Δ_0). This is a well known result which has its origin in the fact that, at zero temperature, all the carriers have condensed into the superfluid and for there to be absorption, two quasiparticle excitations corresponding to the breaking of Cooper pairs out of the condensate are needed. This costs $2\Delta_0$ of energy. In the normal state (dotted curve) the equivalent excitations correspond to the creation of a hole and a particle (2 excitations). At $\omega = 2\Delta_0$ there is a sharp absorption edge and the conductivity jumps to a value close to its normal state Drude value (dotted line in Fig. 1). In the above, the gap has been set at 24 meV, a value characteristic of optimally doped YBCO. Also for the normal state Drude (dotted curve) the impurity scattering rate was $t^+ = 0.001$ meV. This very small value was employed so as to be able to resolve fine structures in the d -wave results which we will now describe.

The dashed line is for a d -wave superconductor in the BCS limit. In the two dimensional CuO_2 Brillouin zone the angle ϕ gives the direction of momentum \mathbf{k} and $\Delta_{\mathbf{k}} = \Delta_0 \cos(2\phi)$ in our simple model. It is clear that, entering into the superconducting state reduces $\sigma_1(\omega)$ in the region of the gap Δ_0 but does not make it go to zero because even at $T = 0$ some of the electrons have zero or very small gap values, namely those on the main diagonals of the Brillouin zone for $\phi = \pm\pi/4$. It is also worth emphasizing that, above $2\Delta_0$ the conductivity goes back to its normal state value faster than it does for the s -wave case. For s -wave the curve for $\sigma_1(\omega)$ is above the normal state Drude for $\omega \geq 2\Delta_0$ and merges with the Drude form from above. For d -wave the superconducting $\sigma_1(\omega)$ is slightly below the Drude in the same region but not by very much. In both cases the missing optical spectral weight on entering the superconducting state, of course, goes into the superfluid which provides a delta

function response in $\sigma_1(\omega)$ at $\omega = 0$. This is not shown in our figure. Note also that the d -wave conductivity has a small structure (on the scale of the figure) at $\omega = \Delta_0$ corresponding to a maximum in slope for $\sigma_1(\omega)$ and has another small structure at $\omega = 2\Delta_0$ corresponding to a kink in the curve. These structures have their origin in the particularities of the d -wave state. For example, in d -wave, the quasiparticle density of states as a function of energy is linear in ω at small ω and has a logarithmic singularity at $\omega = \Delta_0$ before taking on its normal state value at large ω . This singularity is much weaker than for the corresponding s -wave case for which the density of states is zero up to $\omega = \Delta_0$ at which point it displays a inverse square root singularity. This square root singularity does not imply a singularity in $\sigma_1(\omega)$ however. As we have seen in Fig. 1, there is instead only a sharp edge in $\sigma_1(\omega)$ at twice the gap value. We can therefore expect much smaller structures in $\sigma_1(\omega)$ at $\omega = \Delta_0$ and $2\Delta_0$ in d -wave than in the s -wave case at $2\Delta_0$ and this is confirmed by our numerical results given in Fig. 1.

These results are presented here mainly for comparison with full Eliashberg results based on the formalism given in the pervious section which includes inelastic effects. These can be very large in the cuprates, and are described by the charge carrier-mediating-boson spectral density $I^2\chi(\omega)$ introduced in the previous section. Several different theoretical results are presented in Fig. 2. Four different curves are shown for comparison with each other. They were chosen to illustrate the main features present in the in-plane conductivity when inelastic scattering is included. The gray solid line with a maximum before $\omega = 50$ meV are BCS results as in the previous figure. It is totally different from the other curves and disagree strongly with experiment (solid curve). The other curves are all theoretical and based on the Eliashberg equations but with different models for the charge carrier-mediating-boson spectral density $I^2\chi(\omega)$. For the dash-dotted curve referred to as MMP with $\omega_{\text{SF}} = 20$ meV, we employed the simple spectrum for the interaction with the spin fluctuations first introduced by Pines and coworkers.^{46,47} It has the form:^{35,46,47}

$$I^2\chi(\omega) = I^2 \frac{\omega/\omega_{\text{SF}}}{1 + (\omega/\omega_{\text{SF}})^2}, \quad (15)$$

where I^2 is a coupling of the carriers to the spin fluctuations and ω_{SF} is a characteristic

spin fluctuation frequency. In our work I^2 and ω_{SF} are adjusted to get the best possible fit to the normal state conductivity. The same spectrum is used at all temperatures in the superconducting state with the value of g in the $\tilde{\Delta}$ -channel (6a) of the linearized Eliashberg equations set to get the measured value of $T_c = 92.4$ K. There are no other parameters with $g = 0.98$ in Eqs. (6). The resulting dash-dotted curve is to be compared with the BCS result. It is seen to be quite different. In particular there is no trace of the small structures found in the BCS $\sigma_1(\omega)$ at $\omega = \Delta_0$ and $2\Delta_0$. In the MMP model the inelastic scattering at such energies is large and smears out any such small structures. However, now there is a significant structure at Δ_0 plus the energy of the peak in $I^2\chi(\omega)$ namely $\omega_{SF} = 20$ meV. Since in a d -wave superconductor electrons at the Fermi energy with momentum along the main diagonals have zero gap, the boson assisted processes start, in principle, at zero energy plus the boson energy (ω_B) rather than twice the gap plus ω_B . But such processes make only a small contribution to the real part of the conductivity and are not seen as a prominent structure in this quantity. At the gap energy Δ_0 the density of electronic states, however, has a logarithmic van Hove singularity and this is sufficient to produce the structure at $\Delta_0 + \omega_B$ described above. This is discussed in more detail in the work of Carbotte and coworkers^{1,3-7} and we return to it below. It is sufficient here to state that a reasonable picture of the underlying $I^2\chi(\omega)$ can be obtained from a second derivative of the corresponding optical scattering rates as a function of energy. This quantity contains a recognizable picture of $I^2\chi(\omega)$. Here we point out that after the main Drude peak has largely decayed with increasing ω , there is a region of low conductivity in $\sigma_1(\omega)$ which is followed by a rise at higher energies. This rise corresponds to the boson assisted incoherent part of the electron quasiparticle spectral density. The coherent delta function which is also present in the quasiparticle spectral density contributes the Drude. In our work this part contains about 25% of the total spectral weight.

The boson assisted region at higher energies can be used to model $I^2\chi(\omega)$ rather than taking it from some simple theory such as MMP. We can use the solid curve which shows the in-plane data⁷ to get an experimentally measured $I^2\chi(\omega)$. When this is done we find

that it consists of the 41 meV spin resonance measured in inelastic spin polarized neutron scattering experiments, plus a background extending up to 400 meV which we model by an MMP spectrum (15). The resulting $I^2\chi(\omega)$ gives the dashed curve which agrees with the experimental data in the boson region. This good agreement provides strong evidence for charge coupling to the spin resonance at 41 meV which exists only in the superconducting state of optimally doped YBCO² below T_c . The calculations were performed at $T = 10$ K which is close enough to zero. The spectral weight of the spin resonance is largest at $T = 0$ and decreases with increasing T to vanish at $T = T_c$. The temperature dependence of the resonance, measured by neutrons⁸ is also well represented in the optical data.⁷ There are two other sets of results presented in Fig. 2. The dotted curve uses $I^2\chi(\omega)$ in the calculations but also includes impurities in Born scattering with $t^+ = 0.32$ meV. This does not much improve the agreement between theory and experiment in the frequency region below the boson assisted region. The dash-double-dotted curve also includes impurities but this time the unitary limit is used with $\Gamma^+ = 0.63$ meV. We see that we now have an excellent fit to the data throughout the entire frequency range. We note the impurities hardly affect the boson assisted region which determines $I^2\chi(\omega)$ but dominate at low ω and that some resonant scattering must be included to get agreement in this region.

The agreement obtained between Eliashberg theory and experiment is not limited to the real part of $\sigma(\omega)$. In Fig. 3 we show results for the imaginary part of $\sigma(\omega)$, more precisely for $\omega\sigma_2(\omega)$. The curves are labeled as in Fig. 2. The solid line is the data which is not well represented by the dash-dotted curve based on an MMP model for the spectral density. To get agreement it is necessary to include in an Eliashberg calculation the 41 meV resonance as we have done for the real part of $\sigma(\omega)$. The pure case without impurity scattering fits the boson assisted region as well as the other two curves with Born scattering $t^+ = 0.32$ meV (dotted curve) and resonant scattering $\Gamma^+ = 0.63$ meV (dash-double-dotted curve). However, at lower frequencies, below 25 meV, only the curve with resonant scattering fits the data well. Returning to the phonon assisted region the large dip in $\omega\sigma_2(\omega)$ seen around 75-80 meV and reproduced by our theory is a signature of the 41 meV resonance in this quantity. The dip is

not present in a theory of the infrared optical conductivity based on d -wave BCS theory.⁴⁵ In such a theory all structures in $\omega\sigma_2(\omega)$ vs. ω fall around or below twice the value of the gap amplitude Δ_0 . The structure observed in the data at approximately $2\Delta_0$ plus the resonance energy ω_r and is thus the signature of ω_r in $\omega\sigma_2(\omega)$. For the MMP model (dash-dotted curve) there is a dip too but it falls at the wrong energy.

We give a few more details about the second derivative technique which was used by us to construct the underlying spectral density $I^2\chi(\omega)$ from infrared data. A function $W(\omega)$

$$W(\omega) = \frac{1}{2\pi} \frac{d^2}{d\omega^2} \left[\frac{\omega}{\tau(\omega)} \right] \quad (16)$$

is constructed as a guide only. In the normal state and at low temperatures this function is almost exactly^{1,3-7} equal to the input $I^2\chi(\omega)$ for models based on the nearly antiferromagnetic Fermi liquid (NAFFL). Of course, $I^2\chi(\omega)$ is seen in $W(\omega)$ through electronic processes. But in the normal state the electronic density of states $N(\varepsilon)$ is constant and so does not lead to additional structures in $W(\omega)$ that are not in $I^2\chi(\omega)$ which would then corrupt the signal, if the aim is to obtain $I^2\chi(\omega)$ from $W(\omega)$. This is no longer the case in the superconducting state because of the logarithmic van Hove singularities in $N(\varepsilon)$ and these do indeed strongly influence the shape of $W(\omega)$ and introduce additional structures in $W(\omega)$ corresponding to combinations of the positions of the singularity in $N(\varepsilon)$ and the peak in $I^2\chi(\omega)$ at ω_r (resonance frequency) as described by Abanov *et al.*⁴⁸ The structures in $W(\omega)$ corresponding to these singularities contaminate the signal in the sense that $W(\omega)$ in the superconducting state is no longer equal to the input $I^2\chi(\omega)$.^{3,4} In fact, only the resonance peak appears clearly at $\Delta_0 + \omega_r$ and its size in $W(\omega)$ is about twice the value of $I^2\chi(\omega)$ at that frequency. In some cases the tails in $W(\omega)$ also match well the tails in $I^2\chi(\omega)$. In the end, of course, $W(\omega)$ serves only as a guide and it is the quality of the final fit to the conductivity data that determines the quality of the derived $I^2\chi(\omega)$.

Nevertheless, besides giving a measure of the coupling of the charge carriers to the spin resonance $W(\omega)$ can also be used to see the position of density of states singularities, as shown in Fig. 4 where $I^2\chi(\omega)$ (gray squares) and $W(\omega)$ (solid line) derived from our theoretical results are compared. Also shown by vertical arrows are the positions of $\Delta_0 + \omega_r$,

$2\Delta_0 + \omega_r$, $\Delta_0 + 2\omega_r$, and $2\Delta_0 + 2\omega_r$. We note structures at each of these places and this information is valuable. Note that at $2\Delta_0 + \omega_r$ the large negative oscillation seen in $W(\omega)$ is mainly caused by the kink in $I^2\chi(\omega)$ (gray squares) at about 55 meV. The density of electronic states effects clearly distorted the spectrum above the resonance peak and $W(\omega)$ stops agreeing with the input $I^2\chi(\omega)$ in this region until about 150 meV where agreement is recovered. In summary, $W(\omega)$ contains some information on singularities in $N(\varepsilon)$ as well as on the shape and size of $I^2\chi(\omega)$ and, in the superconducting state, the two effects cannot be clearly separated. Nevertheless, $W(\omega)$ remains a valuable intermediate step in the construction of a charge carrier-exchange boson interaction spectral density from optical data.

We next turn to the c -axis dynamics and present results first for a BCS model. To proceed we need to specify the transverse coupling. We have presented in the theory section two possible models. The first one is coherent tunneling with the matrix element $t_\perp(\mathbf{k})$ conserving in-plane momentum and probably equal to $t_\perp \cos^2(2\phi)$ where ϕ is the angle of \mathbf{k} in the two dimensional CuO_2 Brillouin zone. The other model is incoherent tunneling for which momentum is not conserved. To be definite we will use $|V_1/V_0| = 1$ (see Eq. (5)) in the impurity potential. Other values of $|V_1/V_0|$ have been studied by Hirschfeld *et al.*¹⁸ and by others^{25,28} to which the reader is referred for more details.

In Fig. 5 we show BCS results for the real part of the c -axis conductivity $\sigma_{1c}(\omega)$ vs. ω and compare with the in-plane conductivity $\sigma_1(\omega)$ (dotted curve). In this case the gap is 24 meV and the in-plane impurity scattering rate is $t^+ = 0.1$ meV. We see that the structure at Δ_0 and $2\Delta_0$ in the dotted curve for $\sigma_1(\omega)$ have been smeared out somewhat more when compared with the equivalent results shown in Fig. 1. This is due to the larger impurity content. This curve is for comparison with our c -axis results which we now describe. The solid curve is for the coherent tunneling case with $t_\perp(\mathbf{k}) = t_\perp \cos^2(2\phi)$. This hopping probability eliminates the nodal quasiparticles along (π, π) which do not participate in the out-of-plane dynamics. This gets rid of much of the remaining Drude like contribution at very low ω which is still clearly present in the dotted curve although it is substantially reduced by superconductivity

as compared to the normal state Drude (see Fig. 1). The solid curve is small at small ω and peaks just below $\omega \simeq 2\Delta_0$ where the dotted curve for the in-plane case has a small structure. At higher energies, there is little difference between the in-plane and out-of-plane $\sigma_1(\omega)$ although the magnitude of these two quantities is of course very different. If instead of using $t_\perp(\mathbf{k})$ we had used a constant t_\perp for the c -axis transport, the out-of-plane $\sigma_{1c}(\omega)$ would mirror the in-plane case $\sigma_1(\omega)$. This would also hold in the more complex Eliashberg calculations. Only the magnitude is different between in-plane and out-of-plane in this case because of differences in over all multiplicative factors in front of the expression for the conductivity. The final curve in Fig. 5, dash-dotted, is for the incoherent case. We see that it too is near zero at small ω although it rises out of zero more rapidly than does the solid curve. It shows no structure whatever at the gap or at twice its value. The main rise is accomplished within the region $\omega \lesssim 2\Delta_0$. At high ω it saturates to a constant value of one. This is because we have normalized our results to the normal state conductivity and the curve becomes very flat. The corresponding normal state conductivity would be a horizontal line at this saturated value, constant for all ω . This behavior bears no relation to the in-plane coherent result.

The results for $\sigma_{1c}(\omega)$ presented so far are for comparison with those based on solutions for the Eliashberg equations given in the previous section and which properly include inelastic scattering through the spectral density $I^2\chi(\omega)$. Before presenting our c -axis results in this case we stress again that the boson exchange kernel $I^2\chi(\omega)$ is an in-plane quantity and is taken from our discussion of the in-plane conductivity. It is not fitted to any c -axis data. It is to be used unchanged to calculate the out-of-plane conductivity assuming coherent hopping with $t_\perp(\mathbf{k}) = t_\perp \cos^2(\phi)$. The solid curve in Fig. 6 are the in-plane Eliashberg results which are included for comparison with the dashed curve which is for the c -axis. In the boson assisted region, which would not exist in a BCS theory, both curves have a remarkably similar behavior. At very low frequencies, a region which comes mainly from the coherent delta function part of the carrier spectral density, and which is the only part included in BCS, we note a narrow Drude-like peak in the solid curve. This part is suppressed in the c -direction

(dashed curve) because the contribution from the nodal quasiparticles are effectively left out by the $t_{\perp} \cos^2(\phi)$ weighting term. Also, shown for comparison are our previous BCS results for coherent hopping (dotted curve). These results show no resemblance to our Eliashberg results and also do not agree with experiment. What determines the main rise in the region beyond the Drude part of the conductivity in $\sigma_{1c}(\omega)$ are the boson assisted processes and this rise does not signal the value of the gap or twice the gap for that matter but rather a combination of Δ_0 and the resonance energy ω_r .

In Fig. 7 we compare the data from Homes *et al.*¹⁶ on the same graph for in-plane (dotted) and out-of-plane (solid) conductivity $\sigma_1(\omega)$. It is clear that in the c -direction, the nodal quasiparticle seen in the dotted curve are strongly suppressed. This favors the $t_{\perp} \cos^2(2\phi)$ matrix element for the c -axis dynamics as we have just seen. Further, in the boson assisted region the two curves show almost perfect agreement with each other, which again favors the $t_{\perp} \cos^2(2\phi)$ coupling as illustrated in the theoretical curves of Fig. 6. One difference is that the main rise, indicating the onset of the boson assisted incoherent (in-plane) processes, appears to have shifted slightly toward lower frequencies in the c -axis data as opposed to a shift to slightly higher frequencies in our theory. It should be remembered, however, that in the raw c -axis data, large structures appear in the conductivity due to direct phonon absorption and these need to be subtracted out, before data for the electronic background of Fig. 7 can be obtained. In view of this, it is not clear to us how seriously we should take the relatively small disagreements that we have just described between theory and experiment.

With the above reservation kept in mind we show in our last Fig. 8 a comparison of various theoretical results with experimental c -axis conductivity (black solid line). There are five additional curves. The black ones are obtained from an Eliashberg calculation based on the MMP model for $I^2\chi(\omega)$ with impurities $t^+ = 0.32$ meV included to simulate the fact that the samples used are not perfect i.e. are not completely pure, but this parameter does not play a critical role in our discussion. Incoherent c -axis coupling is assumed with $|V_1/V_0| = 1$ (black dotted). It is clear that this curve does not agree with the data and that the coupling along

c cannot be dominated by incoherent hopping between planes. This is also in agreement with the results of a theoretical study by Dahm *et al.*²⁷ who also observed better agreement for coherent c -axis conductivity in the overdoped regime. On the other hand the fit to the black dashed line is good in comparison. It uses the same MMP model but with coherent coupling of the form $t_{\perp}(\mathbf{k}) = t_{\perp} \cos^2(2\phi)$. This fit may already be judged satisfactorily but it should be remembered that if we had used the model of $I^2\chi(\omega)$ with the 41 meV peak included instead of MMP, the agreement would have deteriorated. This is troubling since one would expect that coupling to the 41 meV spin resonance would be stronger in the c -direction data than it is in the in-plane data. This is because the c -axis emphasizes the hot spots around the antinodal directions which connect best to (π, π) in the magnetic susceptibility. This is the position in momentum space where this spin resonance is seen to be located in optimally doped YBCO. On the other hand, recent ARPES data^{41–44} which fit well the MFL (marginal Fermi liquid) phenomenology show little in-plane anisotropy for scattering around the Fermi surface and this is consistent with the findings here.

The dash-dotted curve in Fig. 8 illustrates the fit to the data that can be achieved with a dominant coherent piece and subdominant incoherent contribution. It is not clear to us that such a close fit is significant given the uncertainties in the data and the lack of uniqueness in the fitting procedure. It does, however, illustrate the fact that a small amount of incoherent c -axis hopping cannot be completely ruled out from consideration of the infrared data and that this data can be understood quite well within Eliashberg theory. The last two curves (solid gray and dotted gray) are based on BCS d -wave theory and are reproduced here to illustrate the fact that such a theory is unable to explain the c -axis data. The solid gray curve is with $t_{\perp}(\mathbf{k}) = t_{\perp} \cos^2(2\phi)$ and the dotted gray one for incoherent c -axis transport. Compared with our Eliashberg results the agreement with the data is poor.

IV. CONCLUSION

We have considered the c -axis charge response as revealed in the real part of the frequency dependent optical conductivity $\sigma_{1c}(\omega)$. Results for a pure BCS model, which includes only

elastic impurity scattering, show no agreement with the data in- or out-of-plane. A generalized Eliashberg approach based on a spin fluctuation mechanism leads to much better agreement.

In this approach the coherent delta function like part of the electron spectral density which is sharply peaked at the quasiparticle energy leads to a Drude type response in the normal state and a BCS type response in the superconducting state. The dominant incoherent background of the electron spectral density provided by the coupling to the spin fluctuations, however, leads to an additional boson assisted region for the conductivity which is not strongly changed by the onset of superconductivity except that it is a shift by roughly Δ_0 . This part of the conductivity, not included in BCS, contains the largest part of the optical spectral weight (of order 75%) and can be used to get information on the underlying inelastic processes that presumably cause superconductivity. The in-plane conductivity reveals coupling to the 41 meV resonant peak seen in spin polarized neutron scattering as well as to the spin fluctuation background extending to high energies. For coherent c -axis hopping the boson region in $\sigma_{1c}(\omega)$ has the same form as it does in the in-plane case and this fact is largely born out in the experimental data. This would not be the case if the c -axis coupling were incoherent. Assuming pure incoherent coupling gives no agreement with the data although a best fit is obtained with a small subdominant incoherent part in addition to a dominant coherent part. An important conclusion coming out of our analysis is that the c -axis conductivity data gives independent confirmation for the form of the charge carrier boson spectral density obtained solely from in-plane infrared optical data.

While the infrared conductivity at higher energies is dominated by the inelastic processes and not much affected by a modest amount of elastic impurity scattering, the low energy part is much more sensitive to impurities and depends less directly on inelastic scattering. In this sense, this frequency region can be partly understood within BCS theory at least at low temperatures. One needs to remember, however, that the spectral weight under the Drude-like curve is only a fraction of the entire spectral weight and comes only from the delta function-like part of the electron spectral density. Also, even in this energy region,

there are other profound modifications introduced by the inelastic scattering off the spin fluctuation spectrum. For example all traces of the small structures expected in $\sigma_1(\omega)$ at the gap and twice the gap values are smeared out because, at such higher frequencies, the inelastic scattering rate is already large. Structures do appear in the data, however, at the energy of the gap and of twice the gap plus once or twice the energy of the spin resonance peak which is seen by inelastic neutron scattering at 41 meV in optimally doped YBCO.

Finally, we point out that the spectral density for the excitation spectrum that causes the superconductivity in our approach which consists of a peak at 41 meV plus a long nearly constant background extending to very large energies while consistent with NAFFL of Pines and coworkers,^{46,47} could also arise in other microscopic mechanisms. Recently, the marginal Fermi liquid model, proposed early on,^{41,42} in the development of our understanding of the cuprates, and found to reproduce very well many of the observed anomalous normal state properties, has received new attention because it also fits well the ARPES data. The excitation spectrum of the MFL is quite similar to the one of NAFFL and has many of the features of our empirically determined spectrum provided its normal state version is modified by the 41 meV resonance on entering the superconducting state. In that sense the MFL is equally consistent with optical data. Both, MFL and NAFFL, are phenomenological models having similar excitation spectra associated with the pairing and so cannot easily be distinguished from optics.

ACKNOWLEDGMENT

Research supported by the Natural Sciences and Engineering Research Counsel of Canada (NSERC) and by the Canadian Institute for Advanced Research (CIAR). We thank Dr. C.C. Homes for discussions and for making his data available to us.

REFERENCES

- ¹ J.P. Carbotte, E. Schachinger, and D.N. Basov, *Nature (London)* **401**, 354 (1999).
- ² Ph. Bourges, Y. Sidis, H.F. Fong, B. Keimer, L.P. Regnault, J. Bossy, A.S. Ivanov, D.L. Milius, and I.A. Aksay, in *High Temperature Superconductivity* ed.: S.E. Barnes, *et al.*, CP483 American Institute of Physics, Amsterdam (1999), p. 207-212.
- ³ E. Schachinger and J.P. Carbotte, *Phys. Rev. B* **62**, 9054 (2000).
- ⁴ E. Schachinger and J.P. Carbotte, *Physica C* **341-348** 79-82 (2000).
- ⁵ F. Marsiglio, T. Startseva, and J.P. Carbotte, *Physics Lett.* **A245**, 172 (1998).
- ⁶ F. Marsiglio, *J. of Superconductivity* **12**, 163 (1999).
- ⁷ E. Schachinger, J.P. Carbotte, and D.N. Basov, *Europhys. Lett.* (in print).
- ⁸ P. Dai, H.A. Mook, S.M. Hayden, G. Aeppli, T.G. Perring, R.D. Hunt, and F. Doğan, *Science* **284**, 1344 (1999).
- ⁹ M. Gurvitch, J.M. Valles Jr., A.M. Cucolo, R.C. Dynes, J.P. Garno, L.F. Schneemeyer, and J.V. Waszczak, *Phys. Rev. Lett.* **63**, 1008 (1989).
- ¹⁰ J.W. Loram, K.A. Mirza, and P.F. Freeman *Physics C* **171**, 243 (1990).
- ¹¹ M.R. Norman, M. Randeria, B. Janko, and J.C. Campuzano, *Phys. Rev. B* **61** 14742 (2000).
- ¹² A.M. Zibold, D.B. Tanner, and H. Berger, *Physica B* **244**, 1 (1998).
- ¹³ D.A. Bonn, R. Liang, T.M. Risemann, D.J. Baar, D.C. Morgan, K. Zhang, P. Dosanjh, T.L. Duty, A. MacFarlane, G.D. Morris, J.H. Brewer, W.H. Hardy, C. Kallin, and A.J. Berlinsky, *Phys. Rev. B* **47**, 11314 (1993).
- ¹⁴ M.C. Nuss, P.M. Mankiewich, N.L. O'Malley, and E.H. Westwick, *Phys. Rev. Lett.* **66**, 3305 (1991).

- ¹⁵ M. Matsukawa, T. Mizukoshi, K. Noto, and Y. Shiohara, Phys. Rev. B **53**, R6034 (1996).
- ¹⁶ C.C. Homes, T. Timusk, R. Liang, D.A. Bonn, and W.N. Hardy, Phys. Rev. Lett. **71**, 1645 (1993).
- ¹⁷ S.L. Cooper and K.E. Gray, in: *Physical Properties of High Temperature Superconductors IV*, ed. D.M. Ginsberg, World Scientific, Singapore (1994), p. 61.
- ¹⁸ P.J. Hirschfeld, S.M. Quinlan, and D.J. Scalapino, Phys. Rev. B **55**, 12742 (1997).
- ¹⁹ A. Puchkov, D.N. Basov, and T. Timusk, J. Phys.: Condens. Matter **8**, 10049 (1996).
- ²⁰ P.W. Anderson, in *The Theory of Superconductivity in High- T_c Cuprates*, Princeton University Press, N.J. (1997).
- ²¹ P.W. Anderson, Science **279**, 1196 (1998).
- ²² D.N. Basov, S.I. Woods, A.S. Katz, E.J. Singley, R.C. Dynes, M. Xu, D.G. Hinks, C.C. Homes, and M. Strongin, Science **283**, 99 (1999).
- ²³ A.S. Katz, S.I. Woods, E.J. Singley, T.W. Li, M. Xu, D.G. Hinks, R.C. Dynes, and D.N. Basov, Phys. Rev. B **61**, 5930 (2000).
- ²⁴ L.B. Ioffe and A.J. Millis, Science **285**, 1241 (1999).
- ²⁵ E.H. Kim, Phys. Rev. B **58**, 2452 (1997).
- ²⁶ S. Chakravarty, Eur. Phys. J. B **5**, 337 (1998).
- ²⁷ T. Dahm, D. Manske, and L. Tewordt, Phys. Rev. B **60**, 14888 (1999).
- ²⁸ Winkee Kim and J.P. Carbotte, Phys. Rev. B **61**, R11 886, (2000); Phys. Rev. B **62**, 8661 (2000).
- ²⁹ R.A. Ferrell and R.E. Glover, Phys. Rev. **109**, 1398 (1958); M. Tinkham and R.A. Ferrell, Phys. Rev. Lett. **2**, 331 (1959).
- ³⁰ G. Sandeman and A.J. Schofield, preprint cond-mat/0007299 (unpublished).

- ³¹ T. Xiang and J.M. Wheatley, Phys. Rev. Lett. **76**, 4632 (1996).
- ³² O.K. Anderson, O. Jepsen, A. Lichtenstein, and I.I. Mazin, Phys. Rev. B **49**, 4145 (1994).
- ³³ T. Xiang, C. Panagopoulos, and J.R. Cooper, Intern. J. Mod. Phys. B **12**, 1007 (1998).
- ³⁴ R.J. Radtke, V.N. Kostur, and K. Levin, Phys. Rev. B **53**, R522 (1996).
- ³⁵ E. Schachinger, J.P. Carbotte, and F. Marsiglio, Phys. Rev. B **56**, 2738 (1997).
- ³⁶ E. Schachinger and J.P. Carbotte, Phys. Rev. B **57**, 13 337 (1998).
- ³⁷ B. Stojkovic and D. Pines, Phys. Rev. B **56**, 11931 (1997).
- ³⁸ L.B. Ioffe and A.J. Millis, Phys. Rev. B **58**, 11631 (1998).
- ³⁹ R. Hlubina and T.M. Rice, Phys. Rev. B **51**, 9253 (1995).
- ⁴⁰ D. van der Marel, Phys. Rev. B **60**, R765 (1999).
- ⁴¹ E. Abrahams and C.M. Varma, preprint cond-mat/0003135 (unpublished).
- ⁴² C.M. Varma, P.B. Littlewood, S. Schmidt-Rink, E. Abrahams, and A.E. Ruckenstein, Phys. Rev. Lett. **63**, 1996 (1989); *ibid.* **69**, 497 (1990).
- ⁴³ T. Valla, A.V. Fedorov, P.D. Johnson, B.D. Wells, S.L. Hulbert, G. Li, G.D. Ju, and N. Koshizuka, Science **285**, 2110 (1999).
- ⁴⁴ A. Kamenski, A.J. Mesot, H. Fretwell, J.C. Campuzano, M.R. Norman, M. Randeria, H. Ding, T. Sato, T. Takahashi, T. Mochidu, K. Kadowaki, and H. Hoehst, Phys. Rev. Lett. **84**, 1788 (2000).
- ⁴⁵ I. Schürer, E. Schachinger, and J.P. Carbotte, Physica C **303**, 287 (1998).
- ⁴⁶ A.J. Millis, H. Monien, and D. Pines, Phys. Rev. B **42**, 167 (1990).
- ⁴⁷ P. Monthoux and D. Pines, Phys. Rev. B **47**, 6069 (1993).
- ⁴⁸ Ar. Abanov, A.V. Chubukov, and J. Schmalian, preprint cond-mat/0101220 (unpublished).

FIGURES

FIG. 1. Comparison of the real part of the in-plane conductivity $\sigma_1(\omega)$ of a d -wave superconductor (dashed line) and an s -wave superconductor (solid line). Each have a gap of $\Delta_0 = 24$ meV. For the s -wave there is no absorption till $2\Delta_0$ while for the d -wave with $\Delta_{\mathbf{k}} = \Delta_0 \cos(2\phi)$ with ϕ an angle in the two dimensional Brillouin zone, there is a reduction as compared to the normal state Drude (dotted curve). The slope of $\sigma_1(\omega)$ has a maximum at Δ_0 and $\sigma_1(\omega)$ has an additional small structure at $2\Delta_0$.

FIG. 2. Comparison of the real part of the in-plane conductivity $\sigma_1(\omega)$ vs. ω for various models. The grayed solid line with a peak before 50 meV is BCS. The dash-dotted line is an Eliashberg calculation with an MMP spectral density peaked at $\omega_{\text{SF}} = 20$ meV. The dashed line is the same but with $I^2\chi(\omega)$ used instead of the MMP model. As described in the text this electron-boson spectral density $I^2\chi(\omega)$ has been determined through a consideration of the in-plane optical data. The dotted (Born) and dash-double-dotted (unitary scattering) curves include impurities in addition to the $I^2\chi(\omega)$ model for inelastic scattering. The solid line is the data of Homes *et al.*¹⁶

FIG. 3. The imaginary part of the conductivity $\omega\sigma_2(\omega)$ vs. ω for the various models described in Fig. 2. The solid curve is the data. The dash-dotted curve is the result of an Eliashberg calculation with an MMP model while the other curves are based on the model $I^2\chi(\omega)$ which includes the 41 meV resonance. These three curves are for the pure case (only inelastic scattering, dashed line), and with some additional elastic impurity scattering in Born (dotted) and unitary (dash-double-dotted) limit with $t^+ = 0.32$ meV and $\Gamma^+ = 0.63$ meV respectively.

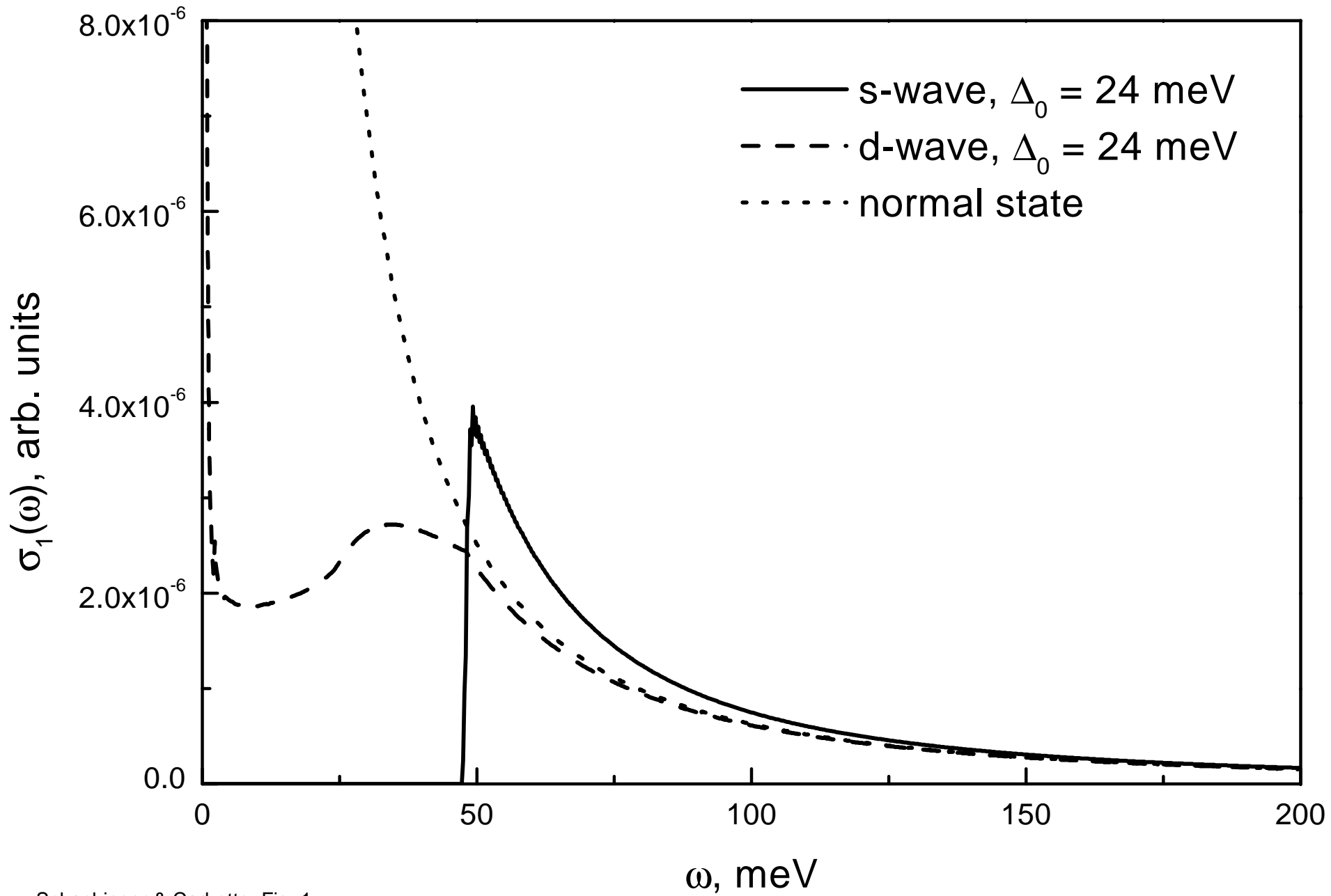
FIG. 4. Second derivative $W(\omega)$ compared with input boson spectral density $I^2\chi(\omega)$. The 41 meV peak in $I^2\chi(\omega)$ (gray squares) is clearly seen in $W(\omega)$ (solid line) as are the tails at higher energies. In the energy region between 75 and 150 meV the van Hove singularities in the electronic density of states show up added on to ω_r and distort the correspondence between $W(\omega)$ and $I^2\chi(\omega)$.

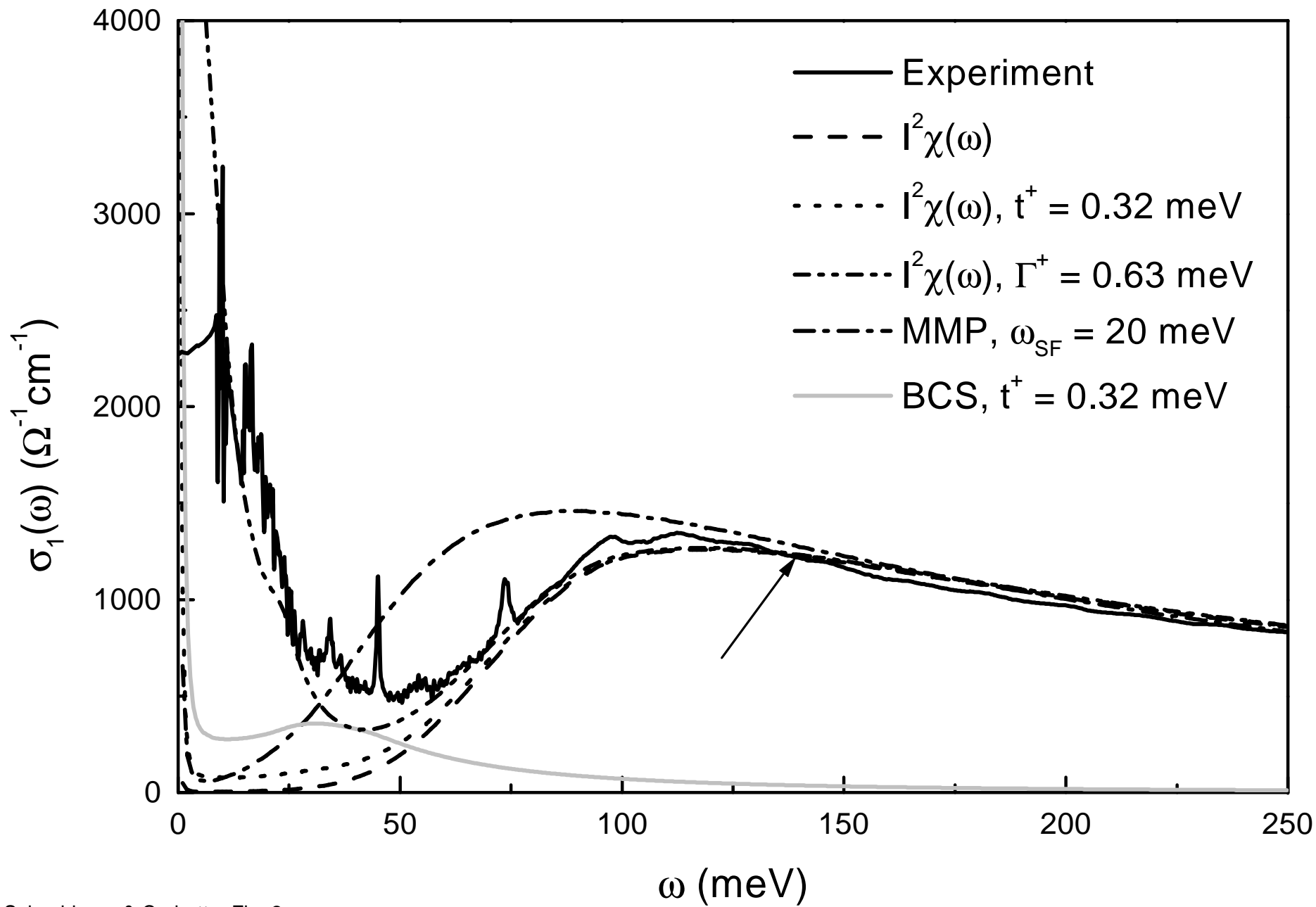
FIG. 5. Comparison of the real part of the conductivity $\sigma_1(\omega)$ vs. ω for the in-plane case (dotted curve) and c -axis. The solid line is for coherent c -axis hopping with $t(\phi) = t_\perp \cos^2(\phi)$ with ϕ an angle in the two dimensional CuO_2 Brillouin zone. The dash-dotted is for incoherent tunneling with $|V_1/V_0| = 1$. All curves are in the BCS model.

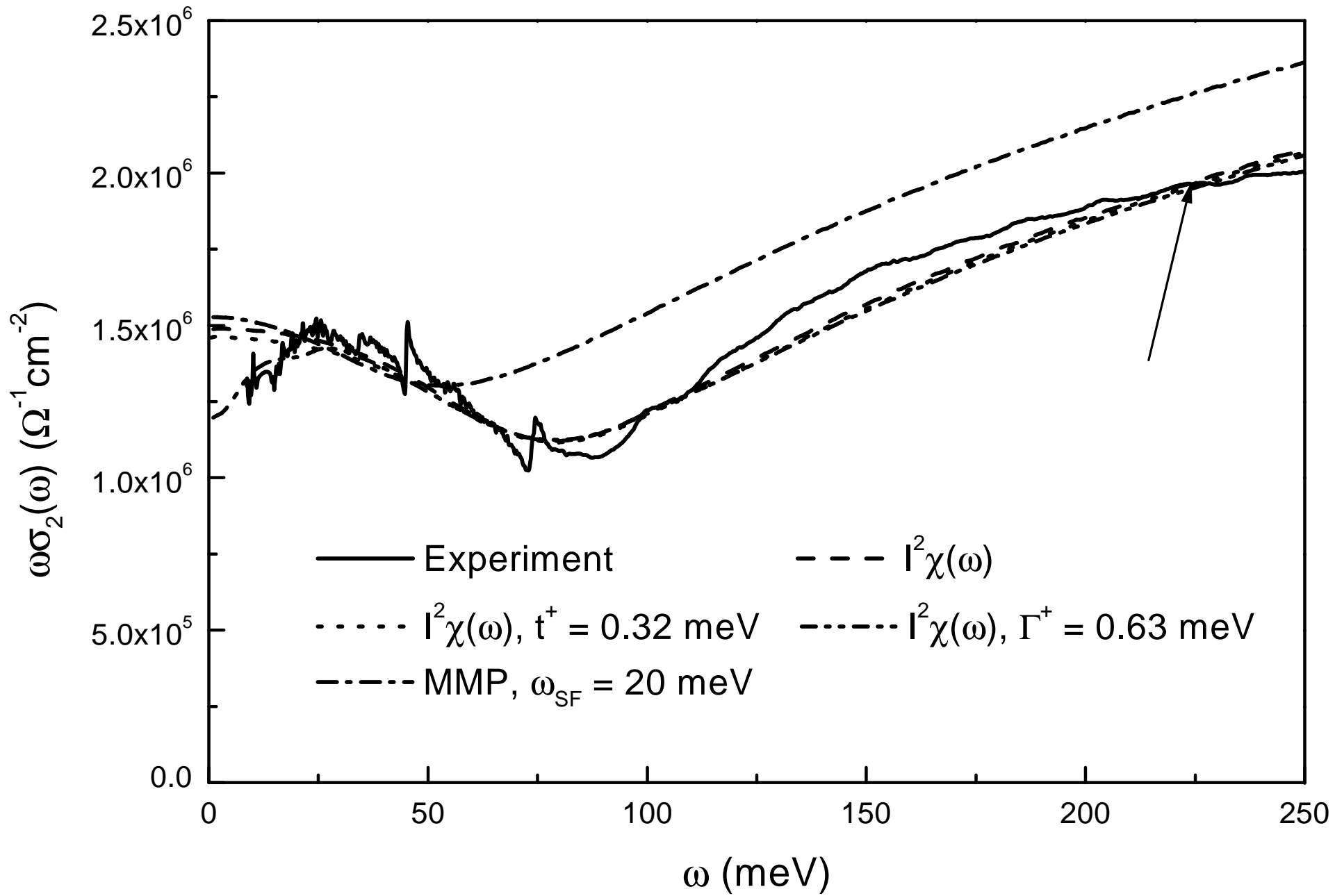
FIG. 6. Comparison between (solid) in-plane and out of plane (dashed) real part of the c -axis conductivity $\sigma_{1c}(\omega)$ vs. ω in an Eliashberg model with our model carrier-boson spectral density $I^2\chi(\omega)$ which includes the 41 meV spin resonance. The dotted curve is $\sigma_{1c}(\omega)$ for a BCS d -wave model with the same gap value as in the Eliashberg work and is included for comparison.

FIG. 7. Comparison between in-plane (dotted) and out of plane (solid) for the real part of $\sigma_1(\omega)$ vs. ω . The data is from Homes *et al.*¹⁶

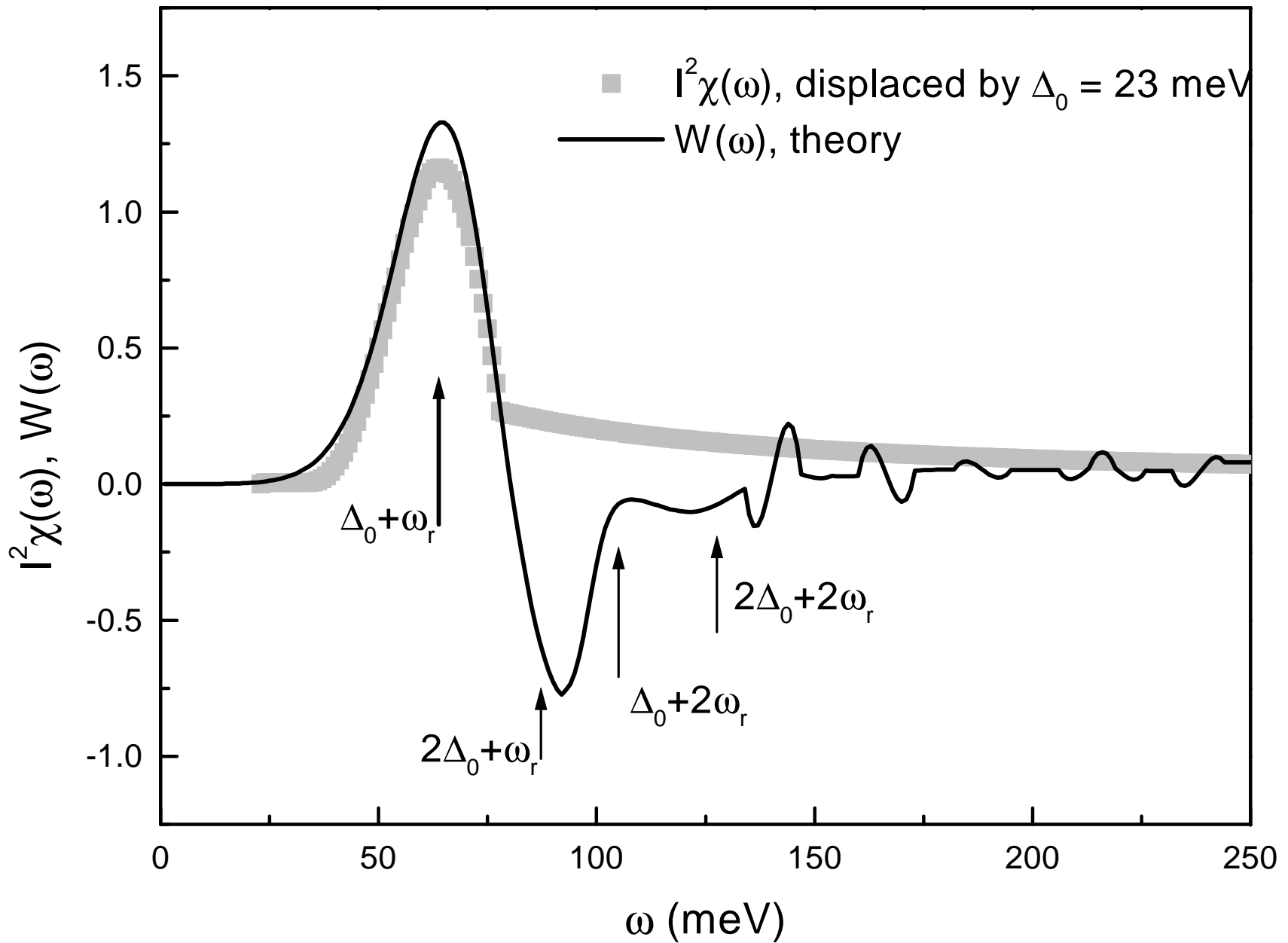
FIG. 8. Comparison with the data of Homes *et al.*¹⁶ for the c -axis conductivity (black solid curve). The theoretical curves were obtained in a BCS theory, solid gray (coherent), dotted gray (incoherent) and the others in Eliashberg theory with MMP model and impurities $t^+ = 0.311$ meV. The black dotted curve is for incoherent c -axis with $|V_1/V_0| = 1$, the dashed for coherent c -axis with $t_\perp(\phi) = t_\perp \cos^2(2\phi)$ with ϕ an angle in the two dimensional CuO_2 Brillouin zone, and the dash dotted is a fit to the data provided by a mixture of coherent and incoherent. We stress that this last fit is for illustrative purposes only, and is not unique.



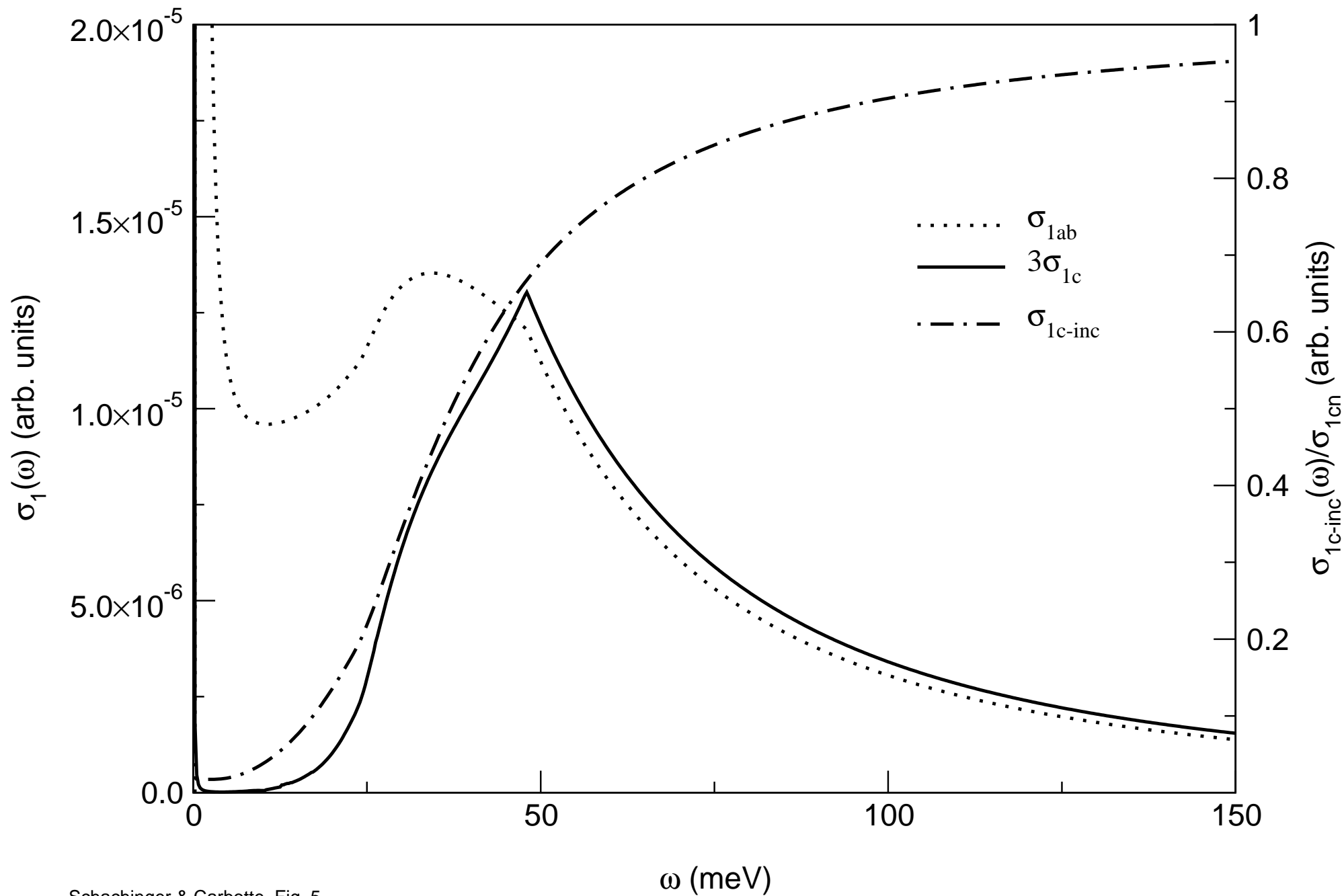


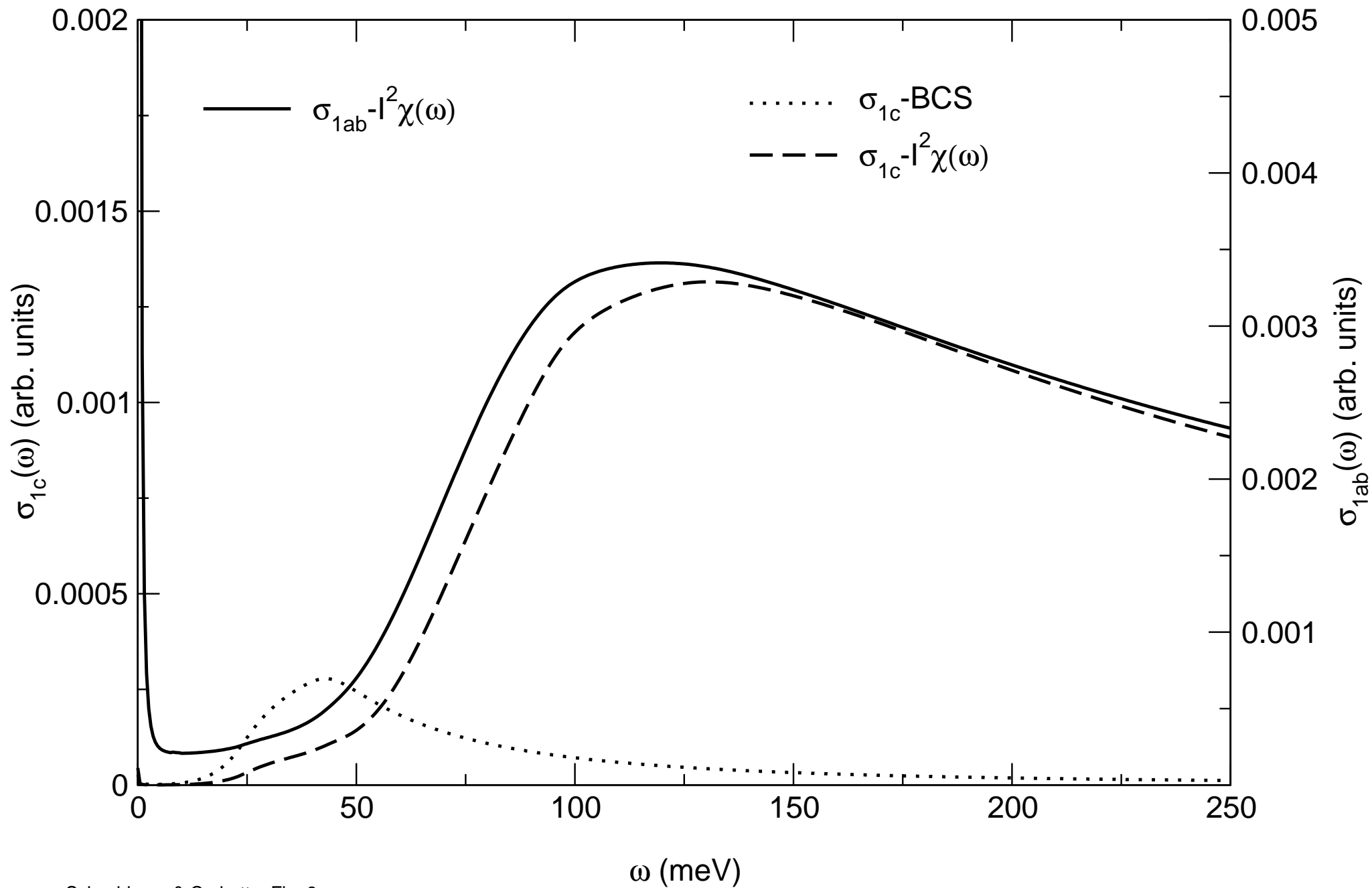


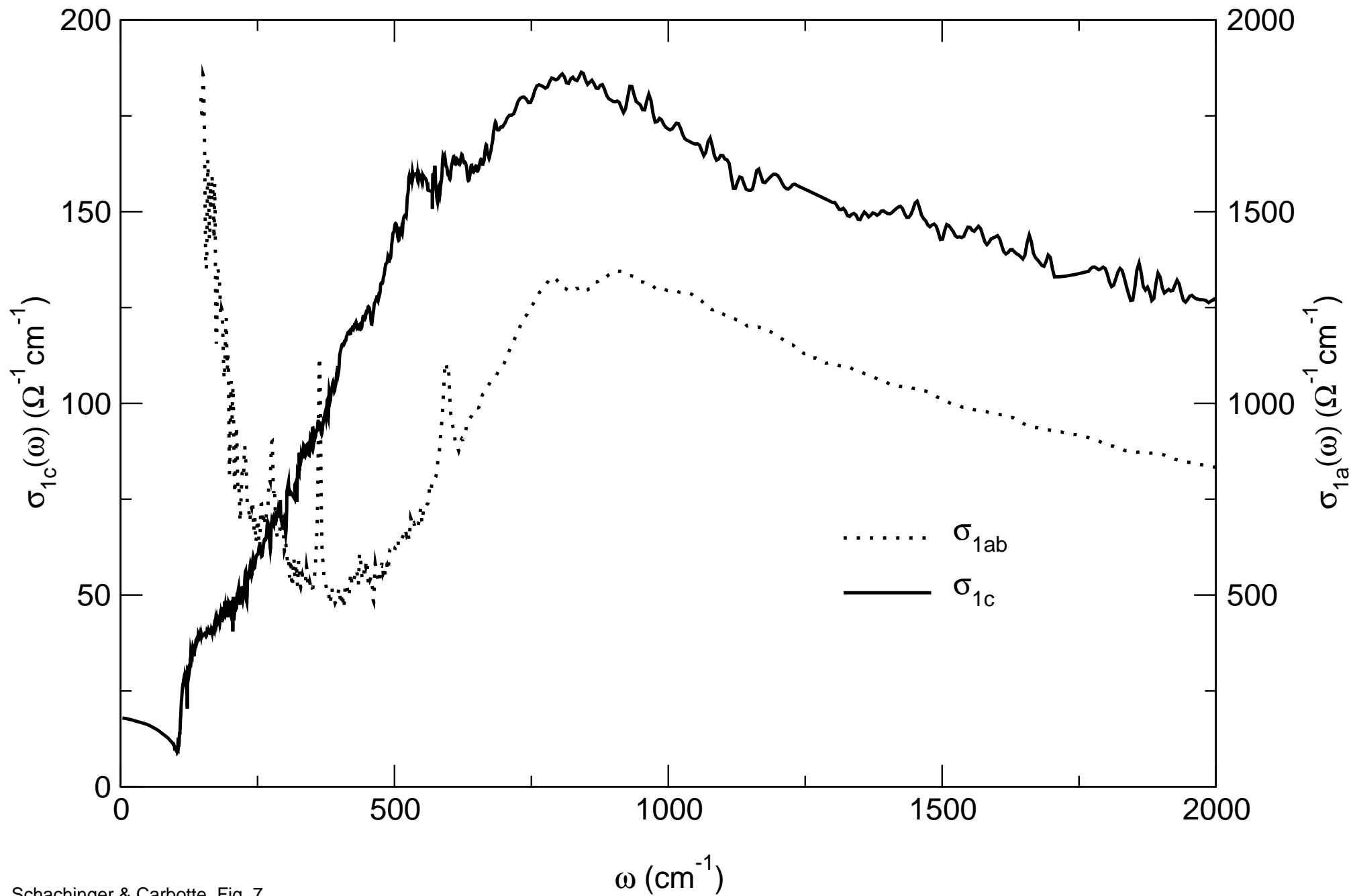
Schachinger & Carbotte, Fig. 3

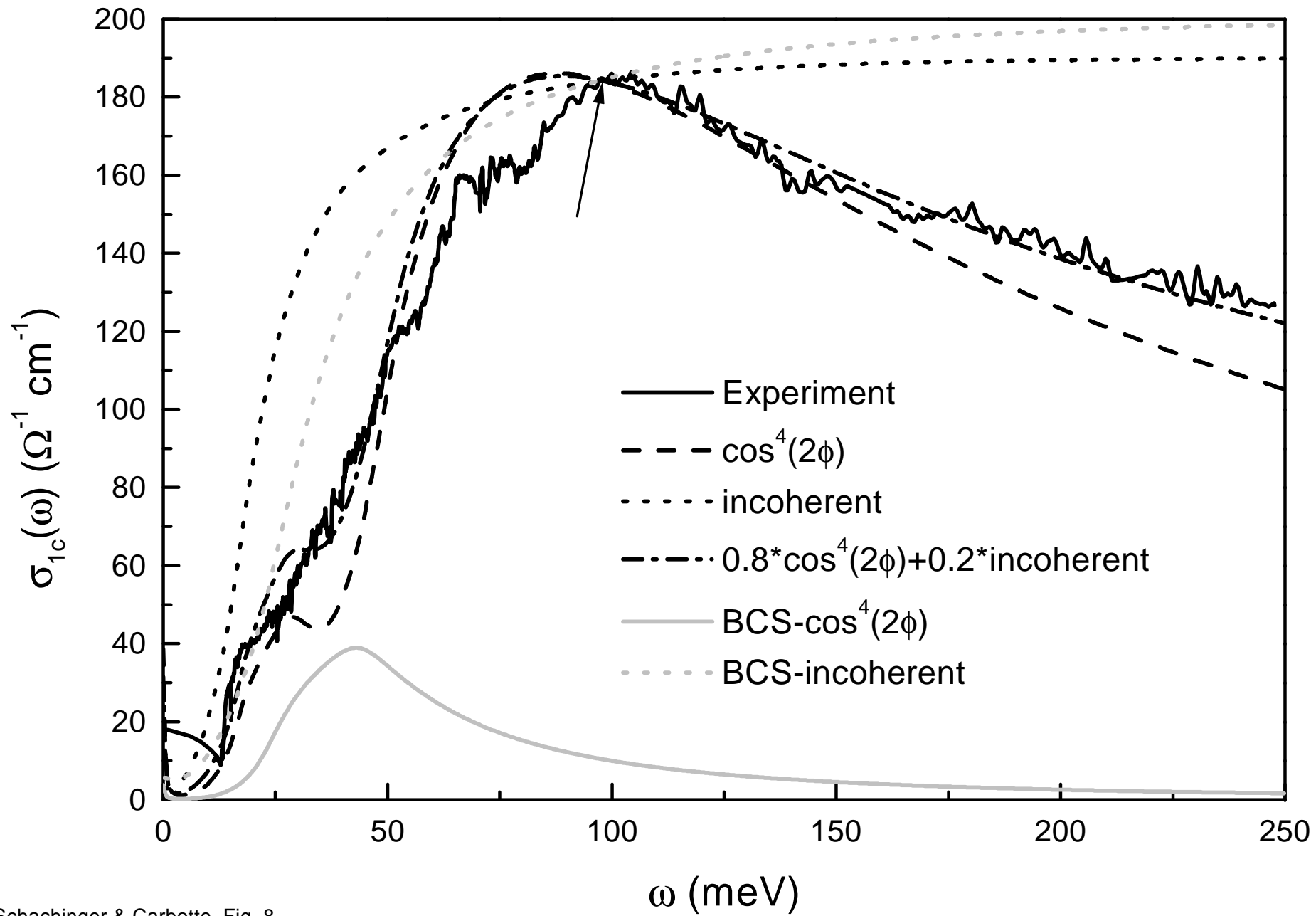


Schachinger & Carbotte, Fig. 4









Schachinger & Carbotte, Fig. 8